J Sustain Const Mater Technol, Vol. 9, Issue. 4, pp. 335–345, December 2024

Journal of Sustainable Construction Materials and Technologies
Web page info: https://jscmt.yildiz.edu.tr
DOI: 10.47481/jscmt.1600562

JSCMT Journal of Sustainable Construction Materials and Technologies

Research Article

Thermophysical, strength, and electrical properties of clay modified with groundnut shell ash for building purposes

Joseph Bassey EMAH[*1], Abayomi Ayodeji EDEMA[2], Sylvester Andrew EKONG[1], David Adeniran OYEGOKE[3], Ubong Williams ROBERT[1], Funke Olawumi FASUYI[4]

[1]*Department of Physics, Akwa Ibom State University, Uyo, Nigeria*
[2]*Department of Geological Sciences, Archivers University, Owo, Nigeria*
[3]*Department of Chemistry, Archivers University, Owo, Nigeria*
[4]*Department of Science Laboratory Technology, Osun State College of Technology, Osun State, Nigeria*

ARTICLE INFO

Article history
Received: 03 June 2024
Revised: 04 November 2024
Accepted: 18 November 2024

Key words:
Abrasion, bulk density, electrical resistance, thermal insulation, water absorption coefficient

ABSTRACT

This study investigated the effects of Groundnut Shell Ash (GSA) on clay samples for making sustainable and low-cost building materials. The clay-GSA composites' physical, chemical, thermal, and mechanical properties were evaluated to assess their suitability for construction. The results revealed that the addition of GSA to the clay matrix had a significant impact on various properties of the samples. The physical characterization showed that GSA was finer and lighter than clay, making the composites more flowable. Chemical analysis indicated that clay and GSA were rich in SiO_2, Al_2O_3, and Fe_2O_3, with the clay exhibiting high SiO_2 content suitable for brick manufacturing. The composites had lower electrical resistance and higher conductivity with more GSA, which could enable temperature monitoring. Thermophysical testing demonstrated that the composites had better thermal insulation properties with more GSA, as shown by higher specific heat capacity and lower thermal diffusivity. The composites absorbed more water with more GSA, indicating higher porosity due to finer particles. The composites had similar bulk density to sandcrete blocks, implying adequate load capacity. Mechanical testing revealed lower flexural strength but higher abrasion resistance with more GSA. The optimal GSA content for strength was 10.0%. More GSA resulted in more voids and weaker bonds. The study provided insights for further research and development.

Cite this article as: Emah, J. B., Edema, A. A., Ekong, S. A., Oyegoke, D. A., Robert, U. W., & Fasuyi, F. O. (2024). Thermophysical, strength, and electrical properties of clay modified with groundnut shell ash for building purposes. *J Sustain Const Mater Technol*, 9(4), 335–345.

1. INTRODUCTION

Humans are blessed with various natural resources, including clay soil, which can be used for multiple applications. However, clay soil needs to be stabilized for shelter construction due to its inherent challenges, such as low strength, high volumetric change, and susceptibility to water damage [1]. One way to overcome these drawbacks is through thermal treatment, which involves firing clay bricks at high temperatures in a kiln [2, 3]. Another effective modification technique is chemical treatment using Portland cement [4, 5]. While these methods can improve the physico-mechanical properties of clay bricks, they also come with potential dangers. Thermal treatment requires high energy and emits carbon dioxide, contributing to environmental issues as a greenhouse gas. Cement dependency is uneco-

***Corresponding author.**
*E-mail address: josephemah@aksu.edu.ng

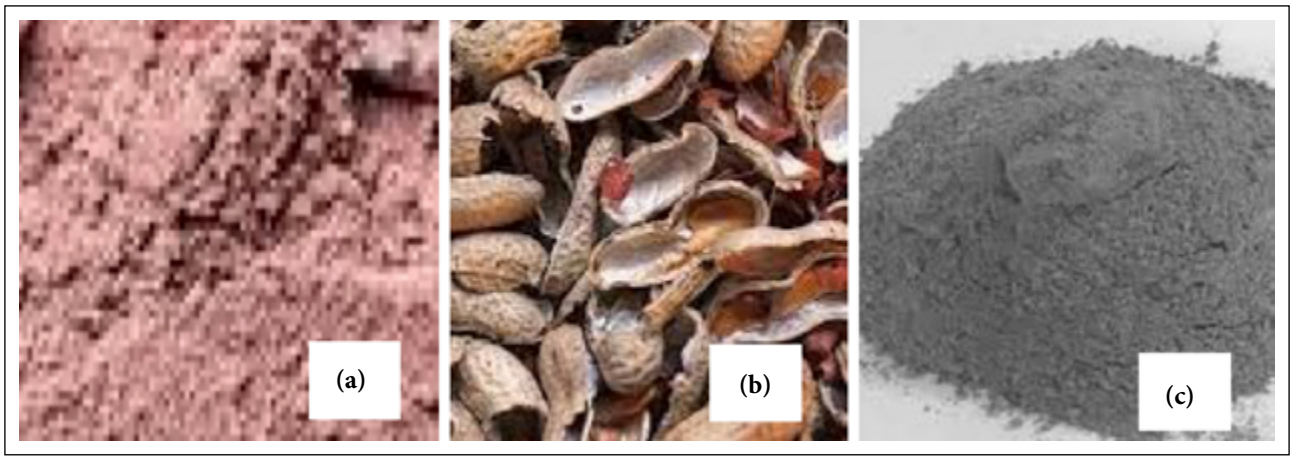

Figure 1. Appearance of **(a)** clay soil, **(b)** groundnut shells, and **(c)** GSA.

nomical due to rising building material costs [6], and the cement industry emits approximately 1.5456 million tons of carbon dioxide into the environment annually [7].

As a result, there has been a growing interest in finding alternative stabilizing agents, mainly focusing on waste valorization for sustainable economic purposes. Realizing that materials with high economic and financial values could be thrown into dustbins [8], man's yearning for the development of industrialization has taken an alarming dimension [9]. Researchers have explored the use of various waste materials, such as textile ash waste [10], rice husk ashes [11], sugarcane bagasse ashes [12], and corn cob ashes [13], which have shown promising potential in improving the properties of clay-based composites compared to cement. Fly ash and slag have also been studied for modifying clay soil with positive results [14–16]. These studies indicate that waste materials can be utilized effectively to enhance clay soil's mechanical and resistance properties for construction.

More so, Ubi et al. [17] treated lateritic soil with groundnut shell ash (GSA) for sub-base material in road construction. They observed that, at 6% content of the GSA, maximum dry density increased from 1.78Mg/m^3 to 2.15Mg/m^3 while the optimum moisture content decreased from 18.5% to 10%. Arthi et al. [18] used GSA to stabilize expansive clay. They found that the investigated properties (maximum dry density, moisture content, and unconfined compression strength) were satisfactory using 10% of the GSA. Sathiparan et al. [19] investigated the density, water absorption rate, compressive, flexural, impact, durability, and thermal characteristics of stabilized earth blocks produced by utilizing GSA. The study's conclusion suggests that the blocks have some promise for significantly reducing the amount of cement needed in the building sector. Sujatha et al. [20] utilized GSA to stabilize locally available highly compressible clay soil and then evaluated consistency limits, compaction characteristics, undrained cohesion, and modulus of elasticity of the soil. They reported that the GSA could be a viable economic alternative in constructing roads and stabilizing soil as a bearing medium.

This study investigates GSA-modified clay materials' thermophysical, strength, and electrical properties to determine their suitability for building purposes. In addition to examining the thermophysical and strength properties, specific electrical properties of the clay-based samples are also evaluated to assess their self-sensing capabilities. Groundnut shells were chosen for this study because they are underutilized and generated in large quantities as waste during groundnut (Arachis hypogaea L.) processing. Ajeigbe et al. [21] noted that groundnut yield could amount to 41.3 million tons from 24.6 million hectares, with China, India, Nigeria, the USA, and Mayaamer as the countries in which it is produced. The shells have been used for various purposes, such as sculpture making [22], biodiesel production [23], heavy metal adsorption [24], and carbon nano-sheet formation [25]. However, improper waste management practices, such as open burning and indiscriminate dumping, have adverse effects on the environment and public health, highlighting the urgent need to address this issue.

2. MATERIALS AND METHODS

2.1. Materials

The primary materials used in this study were groundnut shells, pink clay soil (with a wet and plastic nature), and potable water. These materials were obtained from Uyo Local Government Area of Akwa Ibom State, Nigeria.

2.2. Processing of the Clay and Preparation of Groundnut Shell Ash (GSA)

The clay soil (in small clusters) was spread on a large aluminum tray daily and dried under direct, intense sunlight. Each day, it was weighed after drying, put in a plastic container, and covered correctly. The drying process was discontinued when its weight remained constant for more than five consecutive days of the measurement. The dried clay soil was then crushed using a hammer and screened through a 2-mm sieve. The groundnut shells were soaked in water for 24 hours to remove impurities, followed by complete drying. The dried shells were incinerated in a 20 kW electric furnace at 500 °C for 3 hours to obtain groundnut shell ash (GSA). Figure 1 shows the appearance of the clay soil, groundnut shells, and GSA.

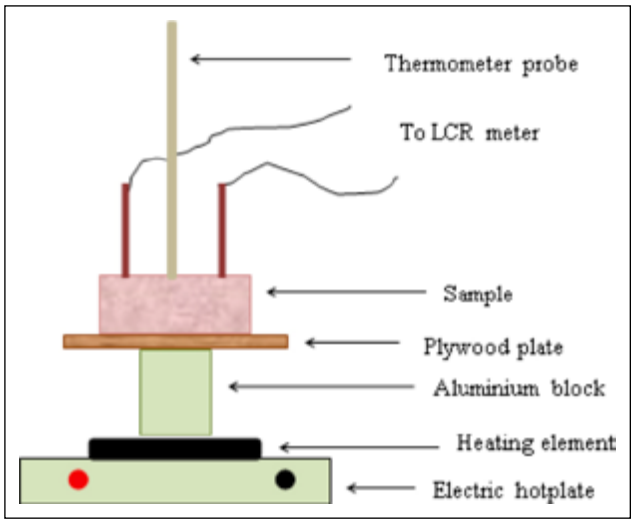

Figure 2. Setup for electrical resistance measurement.

2.3. Analysis of the Processed Materials

The clay and GSA were divided into two portions, with one portion of each material used for analysis. The angle of repose was determined using the fixed funnel method [1]. In this experiment, a material was poured through a plastic funnel onto a predetermined base with known roughness properties. As the material accumulated in a conical shape, the height and radius of the heap were measured within the range of 2.5 cm to 10.0 cm. Seven sets of these measurements were obtained and utilized to create a graph plotting the height against the radius. The angle of repose was then determined by calculating the slope of the graph and applying the inverse tangent rule:

$$\varnothing = \tan^{-1}(S) \quad (1)$$

where $\varnothing$ = angle of repose and S= slope of the graph.

Particle size analysis of the clay was conducted using the hydrometer method of sedimentation according to the standard procedure outlined in [26]. The loose density of the materials was calculated as the ratio of their mass to untapped volume [27]. Using an energy-dispersive X-ray fluorescence spectrometer (Spectro X-lab 2000), the materials were analyzed for chemical composition [28], and their loss on ignition was determined as the decrease in mass during firing [29].

2.4. Sample Fabrication

The remaining portions of each material were used to prepare the samples. Various volume fractions of GSA were considered on an untapped (loose) dry basis. The measured proportions of GSA were added to a fixed clay volume and thoroughly mixed. Moistening of each material mix was carried out using a 1:4 volumetric ratio of water to clay. The resulting mixtures were compacted with a load of 80 kg for 6 hours. Samples for electrical characteristics evaluation were formed into rectangular shapes measuring 50 mm x 28 mm x 15 mm and cured for 18 hours by sprinkling with water for six hours (to keep their surfaces moist) before testing. Two identical copper plates (each with a length of 49 mm and width of 10 mm) were used as electrodes, embedded to a depth of 5 mm and separated by a distance of 35 mm symmetrically from the ends of each sample. Samples for thermophysical property evaluation were developed in circular molds measuring 110 mm in diameter and 7 mm in thickness.

In comparison, samples for strength property examination were formed in molds with dimensions of 220 mm x 33 mm x 14 mm. The samples were fabricated in triplicates for each formulation, and all were dried to constant weight before testing. In this study, the samples were sun-dried for 14 days and then in an electric oven (Model N30C, Genlab) set at 105 °C for about 24 hours. Each sample was weighed before the commencement and at certain intervals during the oven-drying schedule. This oven-drying and weighing process was continuous until no further reduction was noticed in the mass.

2.5. Sample Testing

2.5.1. Electrical Resistance, Temperature Coefficient of Resistance, and Thermal Constant

Figure 2 illustrates this study's setup employed for conducting electrical resistance measurements. A larger thermal insulant, specifically a plywood plate, was utilized to ensure a consistent upward heat flow from the hotplate through the test sample (without heat absorption from the sides). Additionally, an aluminum block (with a height of 80 mm and diameter of 75 mm) was employed to protect the plywood from potential damage caused by direct contact with the heating element.

Before initiating the heating process, the electrodes were adequately insulated with cotton wool. These electrodes were then connected to the probe of an LCR meter (Model No. 9183). Furthermore, a digital thermometer probe was securely clamped to establish firm contact with the top of the sample. The control dial on the hotplate was adjusted to a suitable level for controlling the heat flow.

During the heating process, temperature monitoring and measurement were carried out using the thermometer, and the resistance of the sample was read from the meter at five °C intervals starting from 30 °C. The mean resistance values and their corresponding standard error values were computed for each formulation.

The temperature coefficient of resistance was determined using the following equation:

$$\alpha = \left(\frac{\Delta R}{R_o \Delta T}\right) 100\ \% \quad (2)$$

where α represents the temperature coefficient of resistance, R_o is the electrical resistance at infinity, ΔR is the change in electrical resistance of the sample corresponding to a change in temperature, ΔT.

Furthermore, the value of the thermal constant, β, for each sample was deduced by plotting *ln* R against the inverse of the absolute temperature, T, based on the following relation [30–32]:

$$R = R_o \exp\left[\frac{\beta}{T}\right] \quad (3)$$

where R denotes the mean electrical resistance of the sample.

2.5.2. Water Absorption Coefficient and Bulk Density

The water absorption coefficient of the samples was evaluated using the technique described by Ekong et al. [33]. Figure 3 depicts the experimental setup, where a sample was suspended above water in a transparent vessel using a strong wire. The scale level was adjusted until the sample was submerged approximately 4 mm from its lower end. The timing of water penetration into the sample was initiated, and the mass of the sample was recorded every 15 seconds. At each time interval, the mass of absorbed water (the difference between the dry mass of the sample and the scale reading) was determined. The water absorption coefficient, w, was graphically deduced based on the acquired data using the following relation:

$$w = \frac{M_a}{(A\sqrt{t})} \quad (4)$$

where M_a represents mass of the absorbed water, A is the surface area of the sample through which water vertically penetrates, and t is the duration of water penetration.

Regarding bulk density, a digital weighing scale (S.METTLER - 600 g) was used to measure the mass of each dry sample. The bulk volume was determined using a modified water displacement method [34], and the bulk density was calculated as follows [35, 36]:

$$\rho = \frac{M_s}{V} \quad (5)$$

Where ρ denotes the bulk density of the sample, M_s represents the mass of the sample, and V is the bulk volume of the sample.

2.5.3. Thermal Conductivity

Each sample's thermal conductivity was assessed using the Modified Lee-Charlton's Disc Apparatus Technique, following the methodology described elsewhere [37]. The experimental setup included two identical discs (with a diameter of 110 mm and thickness of 10 mm) and a cylindrical aluminum block, as reported by Robert et al. [38]. An electric hotplate (Lloytron E4102WH) served as the heat source. Before heating, the sample's thickness was insulated with cotton wool. Temperature measurement was performed using two properly calibrated digital thermometers (Model 305) with type-K probes. During each measurement schedule, the control dial of the hotplate was adjusted to enable the temperature of the lower disc to rise and remain at 100 °C. When the steady state was established, the temperature-time data were taken. Origin Software (Version 2019) was utilized to generate temperature-time models based on the data collected during the steady state. The cooling rate of the disc was then determined, and it was used to calculate the thermal conductivity using the equation:

$$k = \left(\frac{Mcx}{A\Delta\theta}\right)\frac{dT}{dt} \quad (6)$$

where k = thermal conductivity of the sample, M = mass of the disc used, c = specific heat capacity of the disc, x = thickness of the sample under test, A = area of the sample's cross-section, Δθ = difference between the temperature of the upper and lower discs at steady state, and $\frac{dT}{dt}$ = cooling rate of the disc.

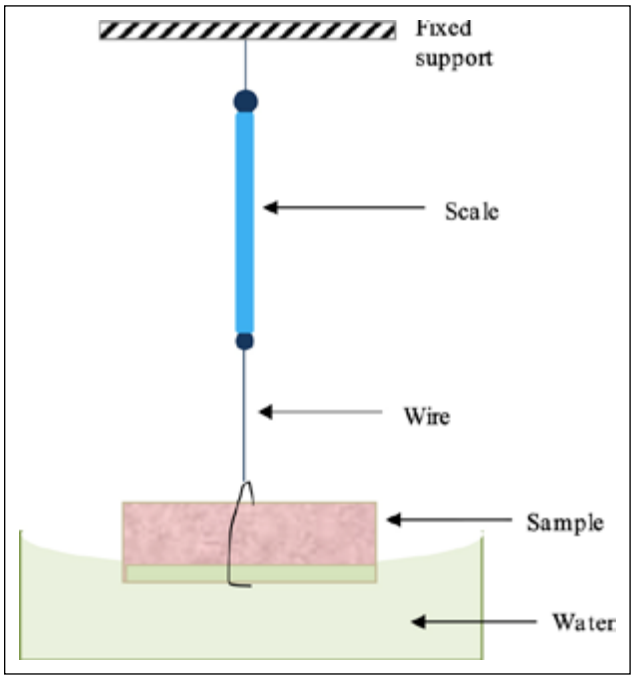

Figure 3. Setup for assessment of water absorption coefficient.

2.5.4. Specific Heat Capacity, Thermal Diffusivity, and Thermal Lag

The specific heat capacity of each sample was determined using SEUR's apparatus [39]. For heat exchange, an aluminum plate and a plywood plate with a thickness of 8 mm were employed as accessories. A square cavity with dimensions 60 mm x 60 mm was created in the center for embedding the accessories. The aluminum plate was heated in an electric oven to approximately 65 °C and quickly sandwiched between the plywood and the sample. During heat exchange, the aluminum plate supplied heat to both the sample and plywood plate, and the temperature of each accessory was monitored. Once thermal equilibrium was reached, assuming the conservation of heat energy, the obtained data were utilized to calculate the specific heat capacity as follows [40]:

$$C = \left(\frac{Q_a - Q_p}{M_s \delta T}\right) \quad (7)$$

where C= specific heat capacity of the sample, Q_a = amount of heat lost by the aluminum plate, Q_p = amount of heat gained by the plywood, M_s = mass of the sample, δT = rise in temperature of the sample.

The values obtained for bulk density, thermal conductivity, and specific heat capacity were utilized to compute the corresponding thermal diffusivity using the equation [41–44]:

$$\lambda = \frac{k}{\rho C} \quad (8)$$

where λ = thermal diffusivity of the sample.

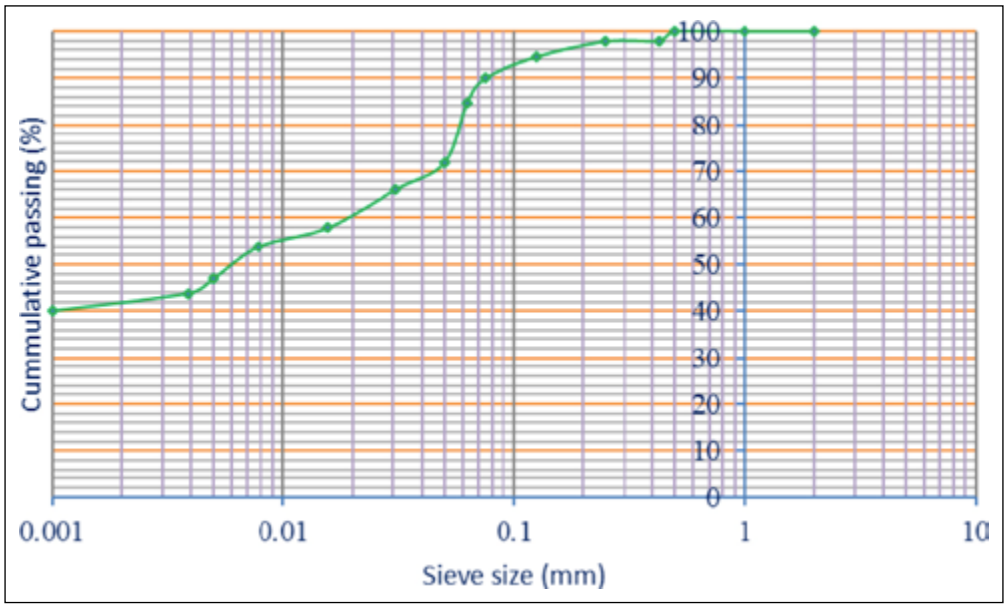

Figure 4. Particle size distribution of the clay soil used.

Furthermore, the thermal lag was calculated on a 24-hour basis using the formula [45]:

$$T_L = \left(\sqrt{\frac{T_p}{4\pi\lambda}}\right) x \quad (9)$$

where T_L = thermal lag of the sample, and T_p = period of the heating cycle.

2.5.5. Abrasion and Flexural Strength

Since the samples may undergo wear during their utilization as building materials, an abrasion test was conducted to predict their durability. During the test, the mass of each sample was recorded, and both surfaces were cleaned using a lint-free cloth. A hard shoe brush was used to rub against the sample surfaces in forward and backward movements for 50 strokes. A 0.5 kg weight was firmly attached to the top of the brush to ensure uniform pressure. The flaked sample was weighed, and the mass of flaking (decrease in sample mass) was determined. The susceptibility to abrasion, A_s, was calculated using the following formula [46]:

$$A_s = \left(\frac{M_f}{M_o}\right) 100\% \quad (10)$$

where A_s= abrasion, M_f = mass of flaking (decrease in the mass of the sample after being flaked), and M_o = mass of the sample before flaking.

Flexural strength investigation used the three-point bending method outlined in ASTM C67/67M [47]. An Electromechanical Universal Testing Machine (WDW-10) was utilized for the test. Each sample was supported at two points on the flexure arrangement of the machine and loaded at its center until failure occurred. At that point, the maximum load applied, F, and the width of the sample, b, were recorded and used to compute the flexural strength, σ, using the following equation [48]:

$$\sigma = \frac{3FL}{2bx^2} \quad (11)$$

Table 1. Description of clay and GSA properties

Parameters	Clay	GSA
Loose density (kgm^{-3})	957.1	235.7
Index of plasticity (%)	23.4	–
Static angle of repose (°)	29.2	36.8

GSA: Groundnut shell ash.

Table 2. The chemical composition of the clay and GSA used

Major oxides		Proportion (%)	
Name	Formula	Clay	GSA
Silica	SiO_2	49.79	49.00
Alumina	Al_2O_3	30.68	12.00
Ferric oxide	Fe_2O_3	6.90	8.20
Lime	CaO	0.74	5.00
Magnesium oxide	MgO	0.21	6.74
Potassium oxide	K_2O	1.87	2.04
Sulphate	SO_3	–	6.21
Loss on ignition	LOI	8.61	4.00

GSA: Groundnut shell ash.

where L = separation of the support points (span length).

For each test, all the samples were evaluated as described in this work, and the mean value for each property was calculated and tabulated along with its corresponding standard error value.

3. RESULTS AND DISCUSSION

Table 1 presents the index properties of the clay and GSA, describing their characteristics. It can be observed that the loose density of GSA is 76.84% lighter than that of the clay. This significant difference suggests that the particles of GSA are smaller compared to those of the clay, as the angle of repose is known to correlate inversely with par-

Table 3. The electrical resistance of the samples at various temperatures

Temperature, T (°C)	Electrical resistance, R(10^3 Ω)based on the GSA proportion in the samples				
	0.0%	10.0%	20.0%	30.0%	40.0%
30.0	876.0±0.3	94.0±0.2	80.6±0.4	72.8±0.3	59.7±0.2
35.0	512.0±0.2	82.1±0.2	59.1±0.3	56.9±0.3	49.7±0.3
40.0	300.0±0.4	74.9±0.4	50.4±0.3	49.0±0.2	40.6±0.2
45.0	198.0±0.2	68.5±0.3	42.8±0.2	40.3±0.4	34.2±0.3
50.0	143.0±0.4	61.2±0.2	38.7±0.2	35.0±0.4	26.4±0.4
55.0	106.0±0.3	52.9±0.3	34.7±0.4	30.9±0.2	21.5±0.3
60.0	71.0±0.3	46.4±0.2	29.0±0.2	25.3±0.3	15.9±0.2

GSA: Groundnut shell ash.

ticle size [49]. Additionally, based on the interpretation of flowability in terms of the angle of repose [50], the obtained values for both the clay and GSA indicate acceptable flow characteristics for manufacturing purposes.

Figure 4 illustrates the clay's gradation, showcasing the particle size distribution. It can be observed that the fraction of sand particles (2 mm–0.06 mm) is the least, followed by silt particles (0.06 mm–2 μm), and finally, clay-sized particles (<2 μm).

Table 2 presents the chemical compositions of the processed materials, clay, and GSA. In that order, both materials are predominantly composed of SiO_2, Al_2O_3, and Fe_2O_3. The clay contains approximately 50% SiO_2, which aligns with the findings of Velasco et al. [51] that clay used in brick factories typically contains 50% to 60% SiO_2. This indicates that the clay material used in this study is suitable for utilization in such factories. For the GSA, the combined proportions of SiO_2, Al_2O_3, and Fe_2O_3 amount to 69.20%. Additionally, the LOI value of the GSA (4.00%) is below the maximum requirement of 6.0%, and the fraction of SO_3 (6.21%) is slightly above 5%. These characteristics signify that the GSA belongs to the class C pozzolanic material according to ASTM C 618 [52].

Table 3 presents the electrical resistance of the developed samples at various temperatures. It can be observed that the electrical resistance of each sample decreases as the temperature increases. This indicates that the samples become more electrically conductive with rising temperatures. The electrical resistance and temperature relationship follows an exponential decay pattern, typical of a negative temperature coefficient (NTC) thermistor (Fig. 5). Robert et al. [53] proposed that this behavior is attributed to the activation energy associated with electron jumping across interfaces in the samples. This phenomenon can be utilized for effective temperature monitoring.

Furthermore, it is noteworthy that the electrical resistance decreases as the proportion of GSA increases in the sample. The inclusion of GSA at a level of 10.0% initiates a significant reduction in the resistance of the clay. The results demonstrate that the resistance of the control clay sample decreases by approximately 89.27%, 90.79%, 91.69%, and 93.18% when incorporating GSA at 10.0%, 20.0%, 30.0%, and 40.0%, respectively, to produce the studied samples. This observation may be attributed to calcium's higher reactivity than aluminum, as the GSA contains a higher proportion of CaO than the clay. Incorporating GSA as a filler in the clay matrix provides the resulting samples with advantages such as low cost, large sensing volume, and the absence of mechanical property loss. These samples exhibit a desirable response to temperature changes and can be applied as walling elements in building construction.

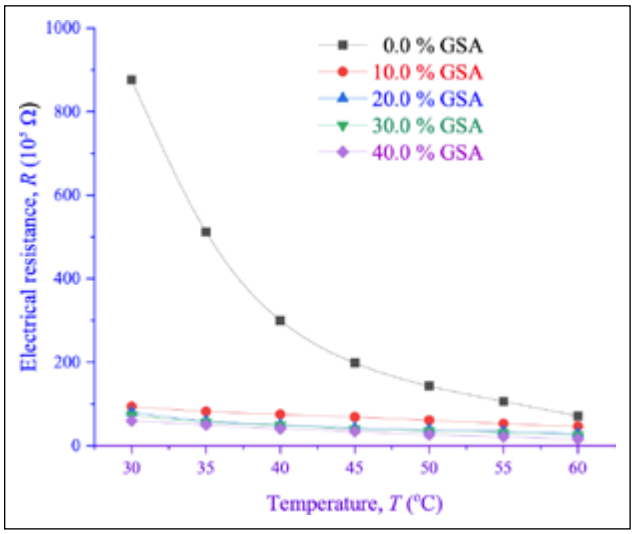

Figure 5. Variation of electrical resistance with temperature of the sample.

Table 4. Temperature coefficient of resistance and Thermal constant of the samples

Proportion of GSA (%)	α (%/°C)	β (K)
0.0	-3.06	8241
10.0	-1.69	2281
20.0	-2.13	3183
30.0	-2.17	3411
40.0	-2.45	4356

GSA: Groundnut shell ash.

Table 4 displays the variations in the temperature coefficient of resistance and thermal constant of the samples with different GSA contents. It can be observed that the inclusion of GSA leads to samples with a higher temperature coefficient of resistance compared to the control sample

Table 5. Thermophysical and strength properties of the samples

Proportion of GSA (%)	w ($kg/m^2 h^{0.5}$)	ρ (10^3 kgm^{-3})	k ($Wm^{-1} K^{-1}$)	C (10^3 $Jkg^{-1} K^{-1}$)	λ (10^{-7} $m^2 s^{-1}$)	T_L (Mins.)	A_s (%)	σ (MPa)
0.0	27.56±0.03	1.662±0.002	0.531±0.004	1.654±0.004	1.93±0.02	22.00±0.09	1.008±0.002	2.894±0.003
10.0	27.14±0.02	1.622±0.004	0.469±0.003	1.671±0.002	1.73±0.01	23.23±0.07	1.024±0.001	2.903±0.002
20.0	28.05±0.04	1.584±0.003	0.436±0.004	1.710±0.004	1.61±0.02	24.14±0.13	1.042±0.002	2.886±0.002
30.0	28.43±0.02	1.568±0.002	0.409±0.006	1.811± 0.002	1.44±0.02	25.49±0.18	1.101±0.002	2.848±0.003
40.0	28.69±0.03	1.549±0.004	0.386±0.005	1.979±0.003	1.26±0.02	27.25±0.18	1.124±0.003	2.799±0.002

GSA: Groundnut shell ash.

(clay sample without GSA content). This indicates an improvement over the control sample, as temperature changes influence a more significant portion of resistance due to incorporating GSA into the clay matrix.

Regarding the values of the thermal constant, it can be inferred that the energy required to enhance electrical conduction is reduced by introducing GSA into the clay matrix. In both cases, the optimal GSA content for achieving the best performance of the samples is 10.0%. With this proportion, the highest temperature coefficient of resistance and the lowest thermal constant values are obtained.

The results of the thermophysical and strength tests conducted on the samples are presented in Table 5. The water absorption coefficient directly correlates with an increasing proportion of GSA. This observation can be attributed to variations in particle sizes between the materials used. Larger particles pack less efficiently, creating larger voids than smaller particles [54]. It has been reported that larger particle sizes result in lower water absorption than smaller ones [55]. These findings lend credence to the water absorption coefficient results in this study, indicating that the GSA particles are finer than those of the clay.

Consequently, as the fraction of GSA increases, the narrowing of the capillary pores is enhanced, thus leading to an increased water absorption coefficient for the samples. However, the value obtained by adding 10% GSA contradicts this assertion, possibly due to the optimal reaction between lime, alumina, and silica in the GSA at that level, enhancing inter-particle packing and micro-aggregation, thereby reducing inter-particle voids. Similar observations were noted in testing clay-based composites containing hydrothermally-calcined waste paper ash materials [1]. Despite the observed variations, all water absorption coefficients obtained in this study fall within the recommended range (20 to 30 $kg/m^2 h^{0.5}$) for solid blocks [33].

The mean bulk density values of the samples exceed the minimum value (1500 kg/m^3) specified for sandcrete blocks made with lightweight aggregates [56] by 3.27% to 10.80%. However, these percentage differences are insignificant, suggesting that the samples could provide a load capacity comparable to that of sandcrete blocks. Samples with 10.0% and 20.0% GSA content exhibit bulk density values similar to those reported for sandcrete blocks with 10% sand partially replaced with untreated coconut husk, cured for 7 days (1575 kg/m^3) and 28 days (1612 kg/m^3) respectively [57]. It is also noteworthy that the thermal conductivity of the samples is slightly lower than the values

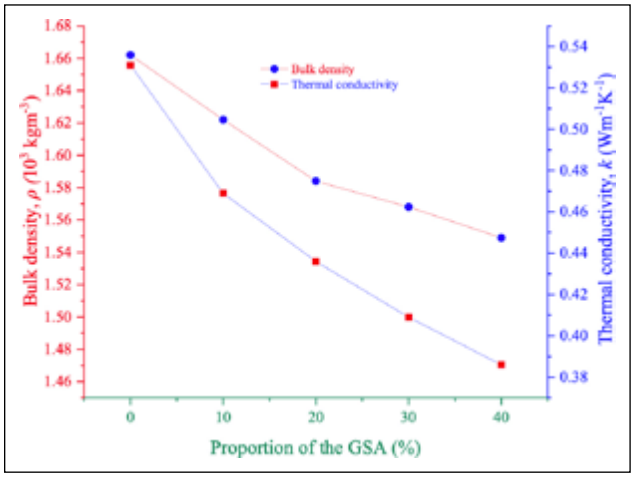

Figure 6. Variation of bulk density and thermal conductivity with proportion of the GSA.

reported for red clay (0.545 W/mK), white clay (0.559 W/mK), and laterite (0.737 W/mK) recommended for passively cooled building designs [58].

Figure 6 illustrates the inverse trends of bulk density and thermal conductivity with the proportion of GSA used. The characteristics of GSA can explain these tendencies. GSA is lighter than the clay soil used in this study, and therefore, an increased proportion of GSA results in a further reduction in the bulk density of the resulting sample. Additionally, incorporating GSA increases the number of pores/voids in the samples. As the samples are dehydrated, the primary phase for thermal energy transmission is the gaseous phase, predominantly filled with air. Since air is a poor heat conductor, the thermal conductivity of the samples decreases as the fraction of GSA increases due to the presence of more air in the samples. This resonates with the assertion that thermal conductivity is a function of bulk density [59].

The improvement in thermal insulation performance of the samples is evident in the higher values of specific heat capacity as the proportion of GSA is increased. With a higher GSA content, the heat-storing ability of a kilogram of the samples is enhanced before a unit change in temperature. This is supported by the observed reduction in thermal diffusivity values as more GSA is incorporated. Thermal diffusivity is directly related to thermal conductivity but is inversely associated with the samples' bulk density and specific heat capacity. By including GSA, thermal conductivity and bulk density are reduced while specific heat capacity is increased.

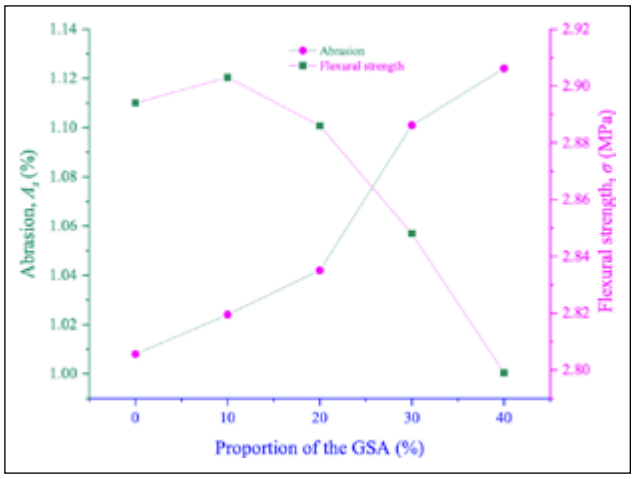

Figure 7. Variation of abrasion and flexural strength with proportion of the GSA.

Consequently, as the proportion of GSA increases, the samples exhibit enhanced resistance to heat transmission and increased demand for heat to effect a change in temperature. This results in a reduced rate of thermal energy diffusion across the thickness of the samples. These tendencies indicate that GSA can improve the thermal insulation of the samples, with a higher proportion of GSA correlating with increased heat-insulating ability. The higher value of thermal lag due to the incorporation of more GSA can be attributed to the trend in thermal diffusivity, suggesting that GSA has the potential to increase the time difference between the maximum temperatures at the outside and inside of the samples when subjected to periodic heating as walling materials in buildings.

The abrasion test results on the samples characterize their flakiness, while the flexural strength values indicate their ability to withstand bending stress during service. A material with a lower abrasion value maintains its original structure and appearance better by resisting mechanical wear [60]. Figure 7 clearly shows that the proportion of GSA influences these properties differently. Abrasion increases with an increasing proportion of GSA as the internal bond between clay particles is weakened by the presence of GSA. However, the effect is not very pronounced, suggesting that the susceptibility to mechanical wear caused by incorporating GSA into the clay matrix may not significantly impact the durability of the clay-modified samples as potential building construction materials.

The chemical composition of GSA highly influences the flexural strength of the samples. During hydration, the chemical phases formed from GSA's calcium, silicates, and aluminate contents play a crucial role in strength development. Specifically, SiO_2 aids in strength development, and in the presence of water, CaO first forms $Ca(OH)_2$, which then yields $CaCO_3$ with the availability of carbon dioxide for hardening and strength development. Flexural strength increases up to a 10% GSA incorporation level, beyond which it progressively declines. This suggests that 10% is the optimum level for achieving maximum strength through the reaction of silica. In other words, as the GSA undergoes a pozzolanic response at a 10% loading level, its silica content dissolves alongside the alumina. It reacts with the calcium hydroxide continuously to form a gel. The presence of water in the process increases the amount of the gel. Since the GSA has finer particles, it is incorporated into the clay matrix as filler. As such, the gel formed can fill the voids in the clay, enhancing particle binding, thereby resulting in a gain of strength by the sample. Further increases in the proportion of GSA lead to excess fractions that are not effectively utilized, resulting in increased void fractions and pores that weaken the inter-particle bonding in the developed composites.

Apart from the fact that the GSA is cheap as a result of being derived from readily available waste material, reliance on GSA for clay stabilization is more economical than dependence on cement. This can be seen in energy consumption (which portrays cost implications if monetary values are considered at a given time). For instance, cement production needs 3.4 GJ of thermal energy (in the wet process) and 110 kWh of electrical power on average, as Afkhami et al. [61] reported. The 20 kW furnace used for 3 hours to prepare the GSA in this study consumes about 216 MJ of electrical energy. It is obvious that even if the production of the GSA is repeated ten times, the total energy consumption would still be less compared to the case with cement.

4. CONCLUSION

In conclusion, this study investigated the properties and performance of clay samples modified with Groundnut Shell Ash (GSA) for potential application as building materials. The key results obtained and deductions drawn from the study can be summarized as follows:

- Physical Properties of the materials: The loose density and angle of repose indicated that the GSA had smaller particle sizes than the clay, making it lighter and more flowable. The particle size distribution of the clay confirmed the presence of sand, silt, and clay-sized particles.
- Chemical Composition: Both the clay and GSA were dominated by SiO_2, Al_2O_3, and Fe_2O_3. The clay contained a high proportion of SiO_2, making it suitable for brick factories. The GSA exhibited pozzolanic properties according to ASTM C 618, making it a potential candidate for construction materials.
- Electrical Resistance: The addition of GSA to the clay matrix significantly reduced electrical resistance. Higher proportions of GSA led to more significant decreases in resistance, with 10.0% GSA content showing the most pronounced effect. This suggests that GSA incorporation can improve electrical conductivity and make the samples suitable for temperature monitoring applications.
- Thermophysical Properties: The thermal insulation performance of the samples improved with increasing proportions of GSA. Specific heat capacity increased while

thermal diffusivity decreased. The highest thermal lag was observed at higher GSA content, indicating a potential for improved energy efficiency and temperature regulation in building applications.

- Water Absorption and Bulk Density: The water absorption coefficient increased with the proportion of GSA, indicating that the GSA particles were finer than the clay. All samples exhibited acceptable water absorption coefficients within the recommended range for solid blocks. Bulk density values were comparable to sandcrete blocks, suggesting that the samples could provide adequate load capacity.
- Flexural Strength and Abrasion Resistance: Flexural strength decreased with increasing GSA content, while abrasion resistance increased. The nature and composition of GSA influenced these properties, with silica playing a crucial role in strength development. Optimum strength was achieved at a 10% GSA incorporation level, beyond which further increases in GSA content weakened the inter-particle bonding and reduced strength.

Based on these results, it can be deduced that adding GSA to clay samples has significant implications for their properties and performance as building materials. The modified samples exhibited improved electrical conductivity, enhanced thermal insulation, and adequate water absorption characteristics. Incorporating GSA also influenced flexural strength and abrasion resistance, with an optimum GSA content of 10.0% yielding the best results.

Overall, this study provides valuable insights into the potential utilization of clay-GSA composites as sustainable and cost-effective materials for construction applications. The findings contribute to understanding their physical, chemical, and thermal properties, paving the way for further research and development in this field.

ETHICS

There are no ethical issues with the publication of this manuscript.

DATA AVAILABILITY STATEMENT

The authors confirm that the data that supports the findings of this study are available within the article. Raw data that support the finding of this study are available from the corresponding author, upon reasonable request.

CONFLICT OF INTEREST

The authors declare that they have no conflict of interest.

FINANCIAL DISCLOSURE

The authors declared that this study has received no financial support.

USE OF AI FOR WRITING ASSISTANCE

Not declared.

PEER-REVIEW

Externally peer-reviewed.

REFERENCES

[1] Robert, U. W., Etuk, S. E., Emah, J. B., Agbasi, O. E., & Iboh, U. A. (2022). Thermophysical and mechanical properties of clay-based composites developed with hydrothermally calcined waste paper ash nanomaterial for building purposes. *Int J Thermophys, 43*(5), 1-20. [CrossRef]

[2] Tsega, E., Mosisa, A., & Fuga, F. (2017). Effects of firing time and temperature on physical properties of fired clay bricks. *Am J Civ Eng, 5*(1), 21-26. [CrossRef]

[3] Rondonane, H. T., Mbeny, J. A., Bayiga, E. C., & Ndjigui, P. D. (2020). Characterization and application tests of kaolinite clays from Aboudeia (Southeastern Chad) in fired bricks making. *Sci Afr, 7*, e00294. [CrossRef]

[4] Garzõn, E., Cano, M., O'Kelly, B. C., & Sãnchez-Soto, P. J. (2015). Phyllite clay-cement composites having improved engineering properties and material applications. *Appl Clay Sci, 114*, 229-233. [CrossRef]

[5] Santos, L. M. A., Neto, J. A. S., & Azerẽdo, A. F. N. (2020). Soil characterisation for adobe mixtures containing Portland cement as a stabiliser. *Revista Matẽria, 25*(1), 1-10. [CrossRef]

[6] Ihuah, P. W. (2015). Building materials costs increases and sustainability in real estate development in Nigeria. *Afr J Econ Sustain Dev, 4*(3), 218-233. [CrossRef]

[7] Dunuweera, S. P., & Rajapakse, R. M. G. (2018). Cement types, composition, uses and advantages of nanocement, environmental impact on cement production, and possible solutions. *Adv Mater Sci Eng, 2018*, 4158682. [CrossRef]

[8] Etuk, S. E., Robert, U. W., Emah, J. B., & Agbasi, O. E. (2021). Dielectric properties of eggshell membrane of some select bird species. *Arab J Sci Eng, 46*, 769-777. [CrossRef]

[9] Etuk, S. E., Agbasi, O. E., Abdulrazzaq, Z. T., & Robert, U. W. (2018). Investigation of thermophysical properties of Alates (swarmers) termites wing as potential raw material for insulation. *Int J Sci World, 6*(1), 1-7. [CrossRef]

[10] Binici, H., Gemci, R., Aksogan, O., & Kaplan, H. (2010). Insulation properties of bricks made with cotton and textile ash wastes. *Int J Mater Res, 101*(7), 894-899. [CrossRef]

[11] Agbede, O., & Joel, M. (2011). Effect of rice husk ash (RHA) on the properties of Ibaji burnt clay bricks. *Am J Sci Ind Res, 2*(4), 674-677. [CrossRef]

[12] Reddy, K. S., Vivek, P. S., & Chambrelin, K. S. (2017). Stabilization of expansive soil using bagasse ash. *Int J Civ Eng Technol, 8*(4), 1730-1736.

[13] Sankar, V. S., Raj, P. D. A., & Raman, S. J. (2019). Stabilization of expansive soil by using agricultural waste. *Int J Eng Adv Technol, 8*(3S), 154-157.

[14] Mandal, S., & Singh, J. P. (2016). Stabilization of soil using ground granulated blast furnace slag and fly ash. *Int J Innov Res Sci Eng Technol, 5*(12), 21121-21126.

[15] Nath, B. D., Molla, M. K. A., & Sarkar, G. (2017). Study on strength behavior of organic soil stabilized with fly ash. *Int Scholarly Res Notices, 2017*, 5786541. [CrossRef]

[16] Dayalan, J. (2016). Comparative study on stabilization of soil with ground granulated blast furnace slag (GGBS) and fly ash. *Int Res J Eng Technol, 3*, 2198-2204. [CrossRef]

[17] Ubi, S. E., Nyak, E. E., & Agbor, R. B. (2022). Enhancement of soil stability with groundnut shell ash. *J Civ Eng Res, 12*(1), 1-7.

[18] Arthi, A. J. J., Aarthi, G., Kumar, V. V., & Vishnupriya, U. (2023). Stabilization of clay using groundnut shell ash and sugarcane bagasse ash. *Key Eng Mater, 960*(1), 197-204. [CrossRef]

[19] Sathiparan, N., Anburuvel, A., Selvam, V. V., & Vithurshan, P. A. (2023). Potential use of groundnut shell ash in sustainable stabilized earth blocks. *Constr Build Mater, 393*, 132058. [CrossRef]

[20] Sujatha, E. R., Dharini, K., & Bharathi, V. (2016). Influence of groundnut shell ash on strength and durability properties of clay. *Geomech Geoeng, 11*(1), 20-27. [CrossRef]

[21] Ajeigbe, H. A., Waliyar, F., Echekwu, C. A., Ayuba, K., Motagi, B. N., Eniayeju, D., & Inuwa, A. (2014). *A farmer's guide to groundnut production in Nigerian*. International Crops Research Institute for the Semi-Arid Tropics.

[22] Sakoalia, K. D., Adu-Agyem, J., Amenuke, D. A., & Deffor, B. (2019). Groundnut shell (powder) as an alternative sculpture material for fine art: The case of Salaga Senior High School, Ghana. *J Arts Humanit, 8*(4), 30-43.

[23] Udeh, B. A. (2018). Bio-waste transesterification alternative for biodiesel production: A combined manipulation of lipase enzyme action and lignocellulosic fermented ethanol. *Asian J Biotechnol Bioresour Technol, 3*(3), 1-9. [CrossRef]

[24] Sowmya, T. A., Gayavajitha, E., Kanimozhi, R., & Subalakshmi, R. (2018). Removal of toxic metals from industrial wastewater using groundnut shell. *Int J Pure Appl Math, 119*(15), 629-634.

[25] Kanokon, N., Andrea, S., & Peter, B. (2018). Influence of KOH on the carbon nanostructure of peanut shell. *Resol Discov, 3*(2), 29-32. [CrossRef]

[26] ASTM D7928. (2017). *Standard test method for particle-size distribution (gradation) of fine-grained soils using the sedimentation (hydrometer) analysis*. ASTM International.

[27] Robert, U. W., Etuk, S. E., Agbasi, O. E., Okorie, U. S., Abdulrazzaq, Z. T., Anonaba, A. U., & Ojo, O. T. (2021). On the hygrothermal properties of sandcrete blocks produced with sawdust as partial replacement of sand. *J Mech Behav Mater, 30*(1), 144-155. [CrossRef]

[28] Bediako, M., & Amankwah, E. O. (2015). Analysis of chemical composition of cement in Ghana: A key to understand the behaviour of cement. *Adv Mater Sci Eng, 2015*, 1-5. [CrossRef]

[29] Inegbenebor, A. I., Inegbenebor, A. O., Mordi, R. C., Kalada, N., Falomo, A., & Sanyaolu, P. (2016). Determination of the chemical compositions of clay deposits from some part of South West Nigeria for industrial applications. *Int J Appl Sci Biotechnol, 4*(1), 21-26. [CrossRef]

[30] Adeniran, A. O., Akankpo, A. O., Etuk, S. E., Robert, U. W., & Agbasi, O. E. (2022). Comparative study of electrical resistance of disc-shaped compacts fabricated using calcined clam shell, periwinkle shell, and oyster shell nanopowder. *Kragujevac J Sci, 44*, 25-36. [CrossRef]

[31] Robert, U. W., Etuk, S. E., Agbasi, O. E., Iboh, U. A., & Ekpo, S. S. (2020). Temperature-dependent electrical characteristics of disc-shaped compacts fabricated using calcined eggshell nanopowder and dry cassava starch. *Powder Metall Prog, 20*(1), 12-20. [CrossRef]

[32] Munifah, S. S., Wiendartun, W., & Aminudim, A. (2018). Design of temperature measuring instrument using NTC thermistor of Fe_2TiO_5 based on microcontroller ATmega 328. *J Phys Conf Ser, 1280*, 022052. [CrossRef]

[33] Ekong, S. A., Oyegoke, D. A., Edema, A. A., & Robert, U. W. (2022). Density and water absorption coefficient of sandcrete blocks produced with waste paper ash as partial replacement of cement. *Adv Mater Sci, 22*(4), 85-97. [CrossRef]

[34] Robert, U. W., Etuk, S. E., & Agbasi, O. E. (2019). Bulk volume determination by modified water displacement method. *Iraqi J Sci, 60*(8), 1704-1710. [CrossRef]

[35] Ekpenyong, N. E., Ekong, S. A., Nathaniel, E. U., Thomas, J. E., Okorie, U. S., Robert, U. W., Akpabio, I. A., & Ekanem, N. U. (2023). Thermal response and mechanical properties of groundnut shells' composite boards. *Res J Sci Technol, 3*(1), 42-57.

[36] Robert, U. W., Etuk, S. E., Ekong, S. A., Agbasi, O. E., Akpan, S. S., & Inyang, N. J. (2023). Paper-sawdust composites: Fabrication and comparison in terms of heat transfer and strength properties. *Struct Environ, 15*(1), 38-48. [CrossRef]

[37] Robert, U. W., Etuk, S. E., Agbasi, O. E., & Okorie, U. S. (2021). Quick determination of thermal conductivity of thermal insulators using a modified Lee-Charlton's disc apparatus technique. *Int J Thermophys, 42*(8), 1-20. [CrossRef]

[38] Robert, U. W., Etuk, S. E., Agbasi, O. E., Okorie, U. S., Ekpenyong, N. E., & Anonaba, A. U. (2022). On the modification of Lee-Charlton's disc apparatus technique for thermal conductivity determination. *Res J Sci Technol, 2*(3), 1-17.

[39] Etuk, S. E., Robert, U. W., & Agbasi, O. E. (2020). Design and performance evaluation of a device for determination of specific heat capacity of thermal insulators. *Beni-Suef Univ J Basic Appl Sci, 9*(1), 1-7. [CrossRef]

[40] Etuk, S. E., Robert, U. W., & Agbasi, O. E. (2022). Thermophysical properties of oil empty fruit bunch peduncle for use as a mulching material. *J Oil Palm Res, 35*, 448-455. [CrossRef]

[41] Etuk, S. E., Robert, U. W., & Agbasi, O. E. (2021). Investigation of heat transfer and mechanical properties of Saccharum officinarum leaf boards. *Int J Energy Water Resour, 6*(1), 95-102. [CrossRef]

[42] Umoren, G. P., Udo, A. O., & Udo, I. E. (2023). Suitability of Lagenaria breviflora rind-filled plaster of Paris ceilings for building design. *Res J Sci Technol, 3*(2), 1-14.

[43] Etuk, S. E., Robert, U. W., Agbasi, O. E., & Ekpo, S. S. (2022). A study on thermophysical properties of clay from Agbani: Its assessment as potential walling material for naturally-cooled building design. *Epitoanyag-J Silicate Based Compos Mater, 74*(3), 93-96. [CrossRef]

[44] Robert, U. W., Etuk, S. E., Agbasi, O. E., Ekong, S. A., Nathaniel, E. U., Anonaba, A. U., & Nnana, L. A. (2021). Valorisation of waste carton paper, melon seed husks, and groundnut shells to thermal insulation panels for structural applications. *Polytechnica, 4*, 97-106. [CrossRef]

[45] Robert, U. W., Etuk, S. E., Agbasi, O. E., Okorie, U. S., & Lashin, A. (2021). Hygrothermal properties of sandcrete blocks produced with raw and hydrothermally-treated sawdust as partial substitution materials for sand. *J King Saud Univ Eng Sci, 2021*, 10.005. [CrossRef]

[46] Robert, U. W., Etuk, S. E., Iboh, U. A., Umoren, G. P., Agbasi, O. E., & Abdulrazzaq, Z. T. (2020). Thermal and mechanical properties of fabricated plaster of Paris filled with groundnut seed coat and waste newspaper materials for structural application. *Építôanyag-J Silicate Based Compos Mater, 72*(2), 72-78. [CrossRef]

[47] ASTM C67/67M. (2021). *Standard test methods for sampling and testing brick and structural clay tile*. ASTM International.

[48] Robert, U. W., Etuk, S. E., Agbasi, O. E., Ekong, S. A., Abdulrazzaq, Z. T., & Anonaba, A. U. (2021). Investigation of thermal and strength properties of composite panels fabricated with plaster of Paris for insulation in buildings. *Int J Thermophys, 42*(2), 1-18. [CrossRef]

[49] Lu, H., Guo, X., Liu, Y., & Gong, X. (2015). Effects of particle size on flow mode and flow characteristics of pulverised coal. *Kona Powder Part I, 32*, 143-153. [CrossRef]

[50] USP. (2007). Powder flow. In *USP 30-NF 25*. United States Pharmacopeial Convention.

[51] Velasco, P. M., Ortíz, M. P. M., Giró, M. A. M., & Velasco, L. M. (2014). Fired clay bricks manufactured by adding wastes as sustainable construction material - A review. *Constr Build Mater, 63*, 97-107. [CrossRef]

[52] ASTM C618. (2023). *Standard specification for coal fly ash and raw or calcined natural pozzolan for use in concrete*. ASTM International.

[53] Robert, U. W., Etuk, S. E., Ekong, S. A., Agbasi, O. E., Ekpenyong, N. E., Akpan, S. S., & Umana, E. A. (2022). Electrical characteristics of dry cement-based composites modified with coconut husk ash nanomaterial. *Adv Mater Sci, 22*(2), 65-80. [CrossRef]

[54] Alssoun, B. M., Hwang, S., & Khayat, K. H. (2015). Influence of aggregate characteristics on workability of superworkable concrete. *Mater Struct, 49*(1), 597-609. [CrossRef]

[55] Kang, M., & Weibin, L. (2018). Effect of the recycled aggregate concrete. *Adv Mater Sci Eng, 2018*, 2428576. [CrossRef]

[56] British Standards Institution. (1975). *BS 2028: Precast concrete blocks*. London.

[57] Robert, U. W., Etuk, S. E., Agbasi, O. E., & Ekong, S. A. (2020). Properties of sandcrete block produced with coconut husk as partial replacement of sand. *J Build Mater Struct, 7*(1), 95-104. [CrossRef]

[58] Ekpe, S. D., & Akpabio, G. T. (1994). Comparison of the thermal properties of soil sample for passively cooled building design. *Turk J Phys, 18*, 117-122.

[59] Robert, U. W., Etuk, S. E., Agbasi, O. E., Umoren, G. P., Akpan, S. S., & Nnanna, L. A. (2021). Hydrothermally-calcined waste paper ash nanomaterial as an alternative to cement for clay soil modification for building purposes. *Acta Polytechnica, 61*(6), 749-761. [CrossRef]

[60] Robert, U. W., Etuk, S. E., Agbasi, O. E., & Umoren, G. P. (2020). Comparison of clay soils of different colors existing under the same conditions in a location. *Imam J Appl Sci, 5*, 68-73. [CrossRef]

[61] Afkhami, B., Akbarian, B., Beheshti, N., Kalaee, A. H., & Shabani, B. (2015). Energy consumption assessment in a cement production plant. *Sustain Energy Technol, 10*, 84-89. [CrossRef]